

The 3d-Electron Heisenberg Pyrochlore $\text{Mn}_2\text{Sb}_2\text{O}_7$

Darren C. Peets,^{1,2,*} Hasung Sim,^{1,2} Maxim Avdeev,³ and Je-Geun Park^{1,2}

¹*Center for Correlated Electron Systems, Institute for Basic Science (IBS), Seoul 08826, Korea*

²*Department of Physics and Astronomy, Seoul National University, Seoul 08826, Korea*

³*Australian Nuclear Science and Technology Organisation, Lucas Heights, NSW 2234, Australia*

In frustrated magnetic systems, geometric constraints or the competition amongst interactions introduce extremely high degeneracy and prevent the system from readily selecting a low-temperature ground state. The most frustrated known spin arrangement is on the pyrochlore lattice, but nearly all magnetic pyrochlores have unquenched orbital angular momentum, constraining the spin directions through spin-orbit coupling. Pyrochlore $\text{Mn}_2\text{Sb}_2\text{O}_7$ is an extremely rare Heisenberg pyrochlore system, with directionally-unconstrained spins and low chemical disorder. We show that it undergoes a spin-glass transition at 5.5 K, which is suppressed by disorder arising from Mn vacancies, indicating this ground state to be a direct consequence of the spins' interactions. The striking similarities to 3d transition metal pyrochlores with unquenched angular momentum suggests that the low spin-orbit coupling in the 3d block makes Heisenberg pyrochlores far more accessible than previously imagined.

Strong frustration, in which interactions compete, impedes spin systems from selecting a unique global ground state at low temperature, leading to a wide variety of physics in which fluctuations, quantum mechanical effects, and fine details of the spin-spin interactions can be crucial[1]. Due to their extremely strong magnetic frustration, pyrochlore oxides and halides host a plethora of exotic phases, such as quantum spin liquids[2–4], or emergent magnetic monopoles[5–7] for classical spins. However, the spins in nearly every known magnetic pyrochlore are either Ising- or XY-like, constrained through spin-orbit coupling to point directly into or out of the tetrahedra on whose corners they reside, or in a plane perpendicular, and in no other direction. Pyrochlore lattices with directionally-unconstrained Heisenberg spins are scarce and not as well studied. With far more degrees of freedom leading to far greater degeneracy, but also a greater ability to adapt to interactions, Heisenberg pyrochlore systems may offer immense potential for unveiling new physics[8].

Spin-orbit coupling, the interaction responsible for coupling spins to the crystal lattice thereby constraining their directions, strengthens as the atomic number increases. Heavy magnetic ions, such as the lanthanides most commonly encountered in the pyrochlore structure, are thus best considered in terms of spin-orbit-coupled j -states linked to the lattice. A comparative lack of pyrochlores containing magnetic ions from earlier in the periodic table, particularly the 3d block, makes pure Heisenberg physics scarce in this lattice. The best-studied 3d-electron pyrochlores, spinel oxides in which the B-site forms a pyrochlore lattice, typically contain Cr^{3+} ($s = 3/2$)[9, 10], whose orbital moments should not be fully quenched and may not behave as pure Heisenberg spins. To the authors' knowledge, only three known materials host pure Heisenberg spins in a pyrochlore lattice: FeF_3 [11, 12], the pyrochlore variant of $\text{Mn}_2\text{Sb}_2\text{O}_7$ (pyr- $\text{Mn}_2\text{Sb}_2\text{O}_7$)[13–15], and recently re-

ported $\text{NaSrMn}_2\text{F}_7$ [16]. All have a high-spin $3d^5$ electron configuration with fully quenched orbital moments, and both FeF_3 and pyr- $\text{Mn}_2\text{Sb}_2\text{O}_7$ are challenging to prepare by conventional solid-state synthesis. Pyrochlore FeF_3 orders magnetically at 22 K[11, 17], a more than 10-fold suppression relative to its less-symmetric and less-frustrated rhombohedral polymorph[18], while the 2.7 K transition in $\text{NaSrMn}_2\text{F}_7$ also indicates very strong frustration. Curiously, pyr- $\text{Mn}_2\text{Sb}_2\text{O}_7$ has been reported to form a spin glass around 41 K[14, 15], several times *higher* than the magnetic transition in its less-frustrated $P3_121$ polymorph[12, 19][20]. With pyr- $\text{Mn}_2\text{Sb}_2\text{O}_7$ having a Curie-Weiss temperature just under 50 K, its putative 41 K transition would correspond to remarkably low frustration in the most-frustrated known three-dimensional magnetic lattice.

In a Heisenberg pyrochlore, the most likely magnetic ground state would be a counterpart of the all-in-all-out state found in Ising pyrochlore antiferromagnets, but the considerable degeneracy could make a variety of other states possible[8], or may prevent long-range order[21, 22]. The lack of purely-Heisenberg systems and the anomalously low frustration in pyr- $\text{Mn}_2\text{Sb}_2\text{O}_7$ have hampered the search for novel physics. We show that the spin glass transition in pyr- $\text{Mn}_2\text{Sb}_2\text{O}_7$ is actually 5.5 K, corresponding to much higher frustration, and this transition is suppressed by Mn vacancies. The Mn^{2+} magnetic ion adopts a $3d^5$ high-spin electronic configuration, with no orbital degree of freedom, leaving the spin directions fully unconstrained. The magnetic behavior is strikingly similar to that in several closely-related 3d pyrochlores having unquenched orbital moments, indicating that the low spin-orbit coupling in the 3d transition metals may render a much broader family of materials as effective Heisenberg pyrochlore systems.

When prepared by conventional solid-state synthesis, $\text{Mn}_2\text{Sb}_2\text{O}_7$ forms in a distorted, chiral variant of the trigonal Weberite structure[19, 23, 24], but the desired py-

rochlore polymorph (Fig. 1a inset) can be stabilized at lower temperatures[13–15]. We prepared powder samples of $\text{pyr-Mn}_2\text{Sb}_2\text{O}_7$ following Brisse[13], with precursor ‘antimonic acid’ prepared from SrCl_5 (Alfa Aesar, 99.997%) and deionized water as in Ref. 25. The precursor was ground with $\text{Mn}(\text{Ac})_2 \cdot 4\text{H}_2\text{O}$ (Aldrich, 99.99%) then reacted for 12h at a sequence of temperatures from 50 to 550°C in Al_2O_3 crucibles in air. Powder diffraction and magnetic measurements were used to verify phase purity and Mn site occupancy.

X-ray powder diffraction patterns were collected using a Bruker D8 Discover diffractometer with a $\text{CuK}\alpha$ source, while a Rigaku Miniflex II was used to collect patterns on precursor ‘antimonic acid’ and monitor reaction completeness. Magnetization measurements were performed in a Quantum Design MPMS-XL magnetometer in RSO measurement mode: a ~ 10 mg powder sample was gently compressed inside a gelatin capsule, which was closed with Kapton tape and inserted into a plastic straw. The sample holder contribution was below the noise level. AC susceptibility was measured in the same magnetometer using the DC sample transport, at zero applied field. Specific heat was measured on a thin plate of pressed powder by the relaxation time method in fields up to 9 T in a Quantum Design PPMS. As an approximate phonon baseline, trigonal Weberite $\text{Sr}_2\text{Sb}_2\text{O}_7$ ceramic prepared by standard solid state synthesis was used. Powder neutron diffraction was performed at the ECHIDNA diffractometer at the OPAL research reactor at ANSTO, Australia, from 6.5 to 164° in steps of 0.05°, with neutron wavelengths of 1.6220 Å (room temperature) and 2.4395 Å (low temperature). Diffraction data were Rietveld-refined in FullProf by the least-squares method[26]. Throughout this paper, molar quantities refer to formula units.

The temperature-dependent DC magnetization of $\text{pyr-Mn}_2\text{Sb}_2\text{O}_7$, shown in Fig. 1, indicates a magnetic transition at $T_f = 5.5$ K, below which the zero-field-cooled and field-cooled magnetization data (Fig. 1a) diverge, implying that the spins order or freeze. This transition broadens and moves to higher temperature in field (Fig. 1c), becoming indistinct above ~ 0.5 T. This is more clearly visible in the derivative (Fig. 1d), which also shows that there is no evidence for any other transition. In particular, the transition reported around 41 K[14, 15] is absent. As shown in Fig. 1b, above ~ 80 K the magnetization obeys the Curie-Weiss law with a Curie-Weiss temperature $T_{\text{CW}} = -49$ K indicating predominantly antiferromagnetic interactions. Deviations from Curie-Weiss behaviour below ~ 80 K indicate the onset of short-range correlations more than an order of magnitude above T_f , while the approximately order-of-magnitude difference between T_{CW} and T_f indicates strong frustration. The paramagnetic moment of $5.59 \mu_B$ is consistent with the spin-only expectation of $5.92 \mu_B$ for high-spin $3d^5$, confirming the absence of an orbital contribution and demon-

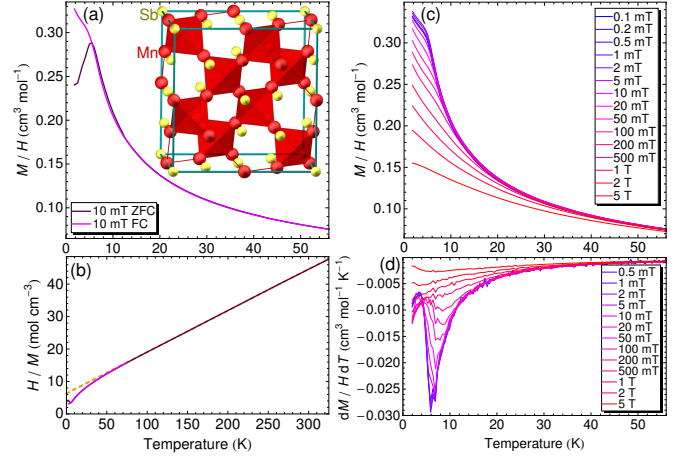


FIG. 1. Magnetization M/H of $\text{pyr-Mn}_2\text{Sb}_2\text{O}_7$. (a) Zero-field-cooled (ZFC) and field-cooled (FC) magnetization in 10 mT, showing a transition at 5.5 K (b) Inverse magnetization, showing a deviation from Curie-Weiss behavior (dashed line) below ~ 80 K. (c) Field-dependence of the FC magnetization. (d) Temperature derivative of the data in (c). The crystal structure is depicted in the inset to (a), with Mn tetrahedra in red and the Sb sublattice in yellow.

strating that $\text{pyr-Mn}_2\text{Sb}_2\text{O}_7$ is indeed a Heisenberg spin system.

The field dependence of the magnetization (Fig. 2a) is S-shaped and exhibits hysteresis at low temperatures, which persists to at least 1.5 T with no clear onset field. The derivative (Fig. 2b) shows clearer evidence of the hysteresis and a lack of any sharp phase transition. Abrupt changes in the hysteresis loops where the field sweep rate was changed indicate strong relaxation effects on the timescale of minutes. To verify this, Fig. 2e shows the results of field-training the sample by cooling to 1.8 K in a 0.1 T field, then monitoring the ensuing magnetization decay after reducing the field to zero. The magnetization is well described by a stretched exponential $M(t) = M_0 + M_R \exp(-(t/t_P)^{1-n})$ [27, 28], with a non-relaxing offset $M_0 = 21.6(2) \text{ cm}^3 \text{ Oe mol}^{-1}$, a substantial relaxing component $M_R = 31.7(14) \text{ cm}^3 \text{ Oe mol}^{-1}$, time scale t_P of 835(112) s, and exponent n of 0.7843(97). An S-shaped hysteresis loop with rate- or time-dependent hysteresis is one key hallmark of a spin glass[27].

The zero-field AC susceptibility χ measured with an excitation amplitude of 1 Oe, shown in Figs. 2(c,d), also shows fingerprints of strong relaxation. A broad peak at low frequencies in the real component χ' agrees well with the magnetization transition, then shifts to significantly higher temperatures as the frequency increases. The imaginary component, χ'' , becomes weakly positive on cooling through the transition, indicating dissipation as the low-frequency measurement field aids the system in finding a ground state. By tracking the frequency dependence of the intrinsic low-temperature transition, the Mydosh parameter $\varphi = \Delta T_N / T_N \Delta \log f = 0.044$

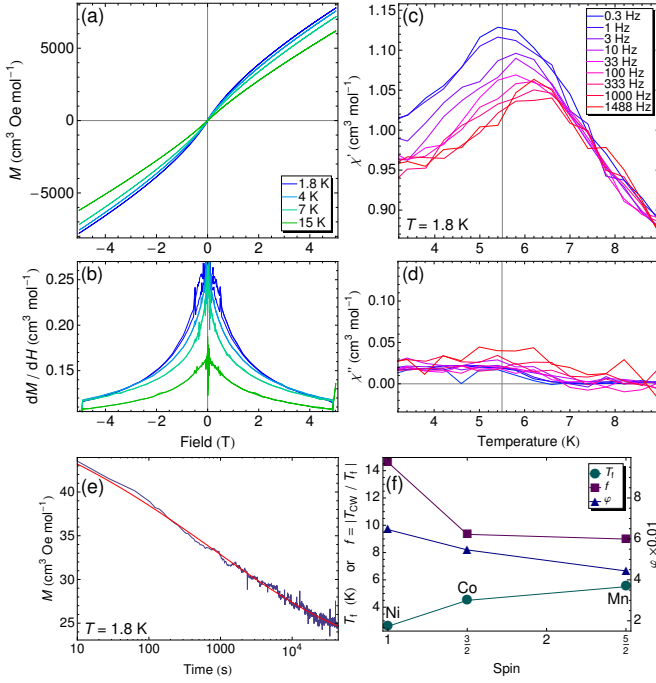


FIG. 2. Magnetic response of pyr-Mn₂Sb₂O₇. (a) $M(H)$ loops; slight hysteresis at 1.8 and 4 K is more evident in (b) the derivative dM/dH . This smooth field and temperature evolution shows no evidence for an abrupt phase transition. Jumps in the derivative correspond to changes in sweep rate. (c) A broad peak in the real part of the zero-field AC susceptibility at $T_f = 5.5$ K, the same temperature identified in $M(T)$, shifts substantially as the drive frequency increases. (d) The loss, χ'' , is weakly positive below the transition. (e) Strong relaxation is visible at 1.8 K. The sample was cooled in a field of 0.1 T, then the field was removed and the zero-field relaxation monitored. (f) Evolution of the intrinsic transitions and frustration in M_2 Sb₂O₇ for M =Ni, Co, Mn, based on Ref. 15.

can be extracted. This is comparable to 0.053 and 0.064 found for pyrochlore Co₂Sb₂O₇ and Ni₂Sb₂O₇, respectively[15], which undergo similar transitions into their low-temperature ground states. The three compounds' progression in transition temperatures, frustration factors $f \equiv |T_{CW}/T_f|$ and Mydosh parameters is plotted in Fig. 2f, based on Ref. 15. Given that the Co and Ni analogs have unquenched orbital moments, the evolution is surprisingly mundane.

The specific heat in Fig. 3 shows a large and very broad hump of magnetic entropy at low temperatures, centered around 2.5 K, roughly half the temperature found *via* magnetization. It does not resemble a usual first- or second-order phase transition, and we have not attempted to extract any more precise estimate for the transition temperature. In applied magnetic fields the hump moves to higher temperatures as does the transition in the magnetization, but it also appears to narrow slightly. Such behavior is readily explained by magnetic field relieving the frustration, and is common in spin

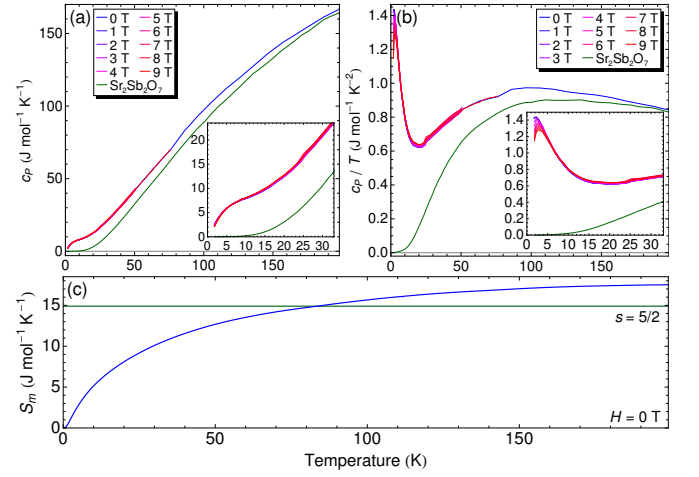


FIG. 3. Specific heat of pyr-Mn₂Sb₂O₇. (a) There is a hump in $c_P(T)$ at low temperatures, and no feature around 41 K. Low-temperature data are highlighted in the inset, and data on Weberite Sr₂Sb₂O₇ serve as a baseline. (b) The broad peak in $c_P(T)/T$ is modified only slightly in field. Magnetic entropy is apparent to at least 40 K. (c) The approximate magnetic entropy calculated by subtracting the Sr₂Sb₂O₇ data. The entropy expected for $s = 5/2$ cannot all be found below ~ 20 K in the c_P/T peak.

glasses. Specific heat data for Sr₂Sb₂O₇[29], a nonmagnetic insulator forming in the related trigonal Weberite structure[30, 31], are included for comparison. However, the phonons in pyr-Mn₂Sb₂O₇ clearly freeze out at significantly lower temperatures, making any subtraction of the phonon background inexact. A very approximate measure of the magnetic entropy can be extracted by subtracting the Sr₂Sb₂O₇ data as a phonon background, but the only conclusion to be drawn here is that most of the entropy expected from $s = 5/2$ $3d^5$ is not released near the transition.

Low-temperature neutron diffraction patterns collected through T_f are shown in Figs. 4a and 4b. The transition introduces no new peaks nor significant changes to the intensities of existing peaks, as further demonstrated by taking the difference across the transition. It is worth noting that there is no low-temperature structural transition that could reduce the frustration. Fig. 4c highlights the presence of a diffuse magnetic component near the (111) nuclear Bragg peak at a d -spacing of ~ 5.8 Å, which becomes indistinct above 20 K, in line with the magnetization and specific heat results. The temperature dependence is shown in Fig. 4d, based on fitting each difference pattern to a Gaussian with a sloping background. pyr-Mn₂Sb₂O₇ now meets all the canonical criteria and has all the earmarks of a spin glass: the ZFC and FC magnetization differ, strong relaxation is observed, the AC susceptibility is strongly frequency dependent, there is only a broad hump below the transition in the specific heat, and long-range order is absent.

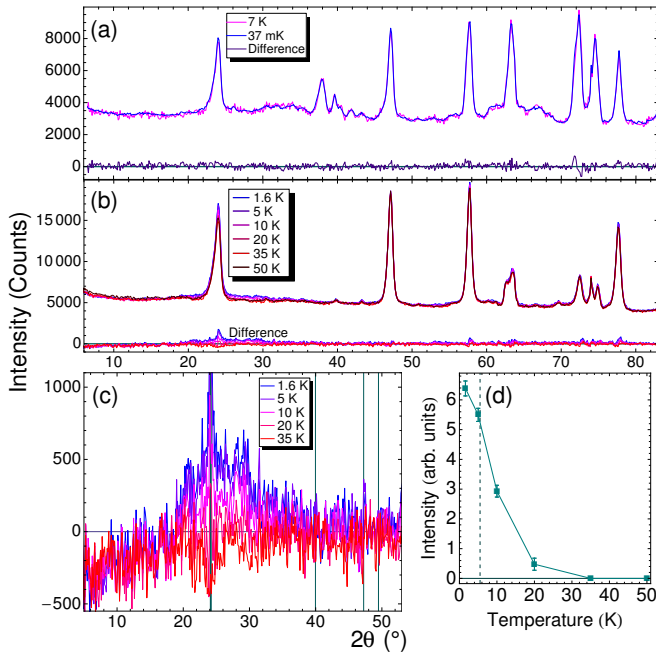


FIG. 4. Low-temperature neutron diffraction on pyr-Mn₂Sb₂O₇. (a, b) Diffraction patterns at low temperature, through T_f , demonstrate the absence of any new magnetic or structural peaks. Differences between 7 K and 37 mK data (a) and from the 50 K data (b) are shown. Several peaks originate from the sample holder — Cu in (a), Al in (b). (c) Difference from data taken at 50 K, highlighting the diffuse contribution. Nuclear Bragg positions are marked. (d) Temperature dependence of the diffuse peak.

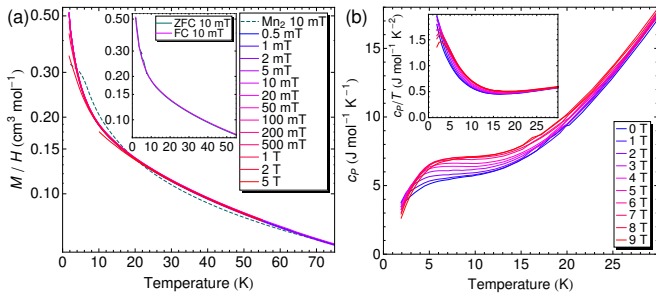


FIG. 5. Properties of Mn-deficient pyr-Mn₂Sb₂O₇. (a) There is no transition in the field-cooled or zero-field-cooled (inset) magnetization. (b) Magnetic fields shift the magnetic entropy to higher temperature.

Mn ions in pyr-Mn₂Sb₂O₇ populate an extremely high-symmetry lattice which should be essentially free from chemical disorder, so there should be nothing extrinsic to the spin system that could locally lock the spins and force a glass transition. Since pyr-Mn₂Sb₂O₇ most likely forms through substituting Mn atoms into the pre-existing pyrochlore matrix of Sb₂O₅ · n H₂O[13], a manganese deficiency is possible and manganese vacancies may be the dominant defect. X-ray diffraction indicated Mn deficiencies in incompletely-reacted material and those pre-

pared from Mn-poor mixtures, but the Mn site refined to full occupancy in all samples reported above. Mn-deficient samples show a significant suppression of T_f , often with no evidence for even the onset of a transition above 1.8 K, but with much stronger field-enhancement in the specific heat — an incompletely-reacted example is shown in Fig. 5. This suppression by disorder strongly suggests that the magnetic freezing is intrinsic. As thermal fluctuations diminish on cooling, it presumably becomes more difficult to rotate any one spin because of the increasing number of spins coupled to it: effectively a diverging mass term. Intriguingly, this behavior is not observed in FeF₃, which enters an all-in-all-out magnetic ground state[18, 32]. The latter has been explained through density functional theory[33], but similar calculations for pyr-Mn₂Sb₂O₇ have not been performed. In FeF₃ nearest-neighbor antiferromagnetic Heisenberg, bi-quadratic, and Dzyaloshinskii-Moriya interactions were all required to adequately model the spin system. In pyr-Mn₂Sb₂O₇, which has a smaller unit cell and rather different ligand coordination, these may be expected to have completely different strengths. In particular, the Mn tetrahedron in pyr-Mn₂Sb₂O₇ contains a central O2 atom, offering a much more direct exchange pathway. Modelling the interactions in this material and the resulting magnetic ground state will be an important avenue for future theoretical exploration.

One important question is why we observe a bulk ordering transition at 5.5 K while previous reports placed it around 41 K[14, 15]. We attribute the previous results to trace quantities of unreacted Mn₃O₄, which has a ferrimagnetic transition around this temperature[34, 35]. Samples which were Mn-rich or incompletely reacted often exhibited a strong transition around 41 K in the magnetization even when phase-pure by x-ray diffraction; however, there was no trace of the transition in the specific heat. Because the Mn₃O₄ ferrimagnetic moments are large and readily field-trained, even trace quantities can dominate the low-field magnetization. This makes it crucial to completely eliminate this impurity if the intrinsic physics of pyr-Mn₂Sb₂O₇ are to be investigated. Previous measurements on pyr-Mn₂Sb₂O₇ display hints of intrinsic behaviour at low temperatures in the inverse magnetization[14], but the data otherwise concentrate, understandably, on the obvious 41 K transition.

In summary, the 3d-electron Heisenberg pyrochlore pyr-Mn₂Sb₂O₇ undergoes a transition around 5.5 K into a spin glass state with dominantly antiferromagnetic interactions. Short-range magnetic correlations survive to much higher temperatures, and strong frustration is evident. The manganese content can be tuned continuously from zero to full occupancy, offering a very interesting control knob for future disorder studies. Measurements to lower temperatures will be required to establish whether the specific heat resembles that in kagome order-by-disorder systems[36–38]. The physical properties of

pyr-Mn₂Sb₂O₇ bear a striking similarity to those of the magnetic pyrochlores Ni₂Sb₂O₇ and Co₂Sb₂O₇[15], and more recently NaSrCo₂F₇, NaCaNi₂F₇, NaCaFe₂F₇, and NaSrFe₂F₇[16, 39, 40], which should all have unquenched orbital moments. This suggests that spin-orbit coupling may be so weak in 3d transition metal pyrochlores as to be effectively irrelevant to the frustrated spins, greatly broadening the suite of materials available for investigating effective Heisenberg physics on the most frustrated known three-dimensional lattice. The very recently reported NaSrMn₂F₇[16], with quenched orbital moments but A-site cation disorder, also behaves in a similar manner.

This work was supported by the Institute for Basic Science (IBS) in Korea (IBS-R009-G1). The authors are indebted to M. Gingras for stimulating discussions. We acknowledge the support of the Bragg Institute, Australian Nuclear Science and Technology Organisation, in providing neutron research facilities used in this work.

* Current address: State Key Laboratory of Surface Physics, Department of Physics, and Advanced Materials Laboratory, Fudan University, Shanghai 200438, China

- [1] C. Lacroix, P. Mendels, and F. Mila, eds., *Introduction to Frustrated Magnetism*, Springer Series in Solid-State Sciences, Vol. 164 (Springer, Berlin, 2011).
- [2] J. S. Gardner, M. J. P. Gingras, and J. E. Greedan, *Rev. Mod. Phys.* **82**, 53 (2010), arXiv:0906.3661 [cond-mat.dis-nn].
- [3] L. Balents, *Nature* **464**, 199 (2010).
- [4] K. A. Ross, L. Savary, B. D. Gaulin, and L. Balents, *Phys. Rev. X* **1**, 021002 (2011), arXiv:1107.0761 [cond-mat.str-el].
- [5] C. Castelnovo, R. Moessner, and S. L. Sondhi, *Nature* **451**, 42 (2008), arXiv:0710.5515 [cond-mat.str-el].
- [6] D. J. P. Morris, D. A. Tennant, S. A. Grigera, B. Klemke, C. Castelnovo, R. Moessner, C. Czternasty, M. Meissner, K. C. Rule, J.-U. Hoffmann, K. Kiefer, S. Gerischer, D. Slobinsky, and R. S. Perry, *Science* **326**, 411 (2009), arXiv:1011.1174 [cond-mat.mtrl-sci].
- [7] T. Fennell, P. P. Deen, A. R. Wildes, K. Schmalzl, D. Prabhakaran, A. T. Boothroyd, R. J. Aldus, D. F. McMorrow, and S. T. Bramwell, *Science* **326**, 415 (2009), arXiv:0907.0954 [cond-mat.mtrl-sci].
- [8] Y. Wan and M. J. P. Gingras, “Color ice states, weathervane modes, and order by thermal disorder in the bilinear-biquadratic pyrochlore heisenberg antiferromagnet,” (2016), arXiv:1607.02185 [cond-mat.str-el].
- [9] S.-H. Lee, C. Broholm, W. Ratcliff, G. Gasparovic, Q. Huang, T. H. Kim, and S.-W. Cheong, *Nature* **418**, 856 (2002), arXiv:cond-mat/0208587 [cond-mat.str-el].
- [10] K. Tomiyasu, H. Suzuki, M. Toki, S. Itoh, M. Matsuura, N. Aso, and K. Yamada, *Phys. Rev. Lett.* **101**, 177401 (2008), arXiv:0804.2993 [cond-mat.str-el].
- [11] R. De Pape and G. Ferey, *Mater. Res. Bull.* **21**, 971 (1986).
- [12] J. N. Reimers, J. E. Greedan, C. V. Stager, M. Björgvinnsen, and M. A. Subramanian, *Phys. Rev. B* **43**, 5692 (1991).
- [13] F. Brisse, D. J. Stewart, V. Seidl, and O. Knop, *Can. J. Chem.* **50**, 3648 (1972).
- [14] H. D. Zhou, C. R. Wiebe, A. Harter, N. S. Dalal, and J. S. Gardner, *J. Phys.: Condens. Matter* **20**, 325201 (2008).
- [15] H. D. Zhou, C. R. Wiebe, J. A. Janik, B. Vogt, A. Harter, N. S. Dalal, and J. S. Gardner, *J. Solid State Chem.* **183**, 890 (2010).
- [16] M. B. Sanders, J. W. Krizan, K. W. Plumb, T. M. McQueen, and R. J. Cava, “NaSrMn₂F₇, NaCaFe₂F₇, and NaSrFe₂F₇: novel single crystal pyrochlore antiferromagnets,” (2016), arXiv:1608.02907 [cond-mat.str-el].
- [17] Y. Calage, M. Zemirli, J. Greneche, F. Varret, R. De Pape, and G. Ferey, *J. Solid State Chem.* **69**, 197 (1987).
- [18] G. Ferey, R. DePape, M. Leblanc, and J. Pannetier, *Rev. Chim. Miner.* **23**, 474 (1986).
- [19] D. C. Peets, H. Sim, S. Choi, M. Avdeev, S. Lee, S. J. Kim, H. Kang, D. Ahn, and J.-G. Park, “Magnetic transitions in the chiral armchair-kagome system Mn₂Sb₂O₇,” (2016), arXiv:1611.02372 [cond-mat.str-el].
- [20] The *P*3₁21 polymorph of Mn₂Sb₂O₇ consists of alternating kagome and triangular Mn layers, as in the pyrochlore structure, but shifted to produce a very different, chiral, structure. A detailed study on the *P*3₁21 polymorph is presented elsewhere[19].
- [21] R. Moessner and J. T. Chalker, *Phys. Rev. Lett.* **80**, 2929 (1998), arXiv:cond-mat/9712063 [cond-mat.stat-mech].
- [22] R. Moessner and J. T. Chalker, *Phys. Rev. B* **58**, 12049 (1998), arXiv:cond-mat/9807384 [cond-mat.stat-mech].
- [23] H. G. Scott, *J. Solid State Chem.* **66**, 171 (1987).
- [24] L. Chelazzi, T. B. Ballaran, G. O. Lepore, L. Bindi, and P. Bonazzi, *Solid State Sci.* **21**, 85 (2013).
- [25] D. J. Stewart and O. Knop, *Can. J. Chem.* **48**, 1323 (1970).
- [26] J. Rodríguez-Carvajal, *Physica B* **192**, 55 (1993).
- [27] J. A. Mydosh, *Hyperfine Interactions* **31**, 347 (1986).
- [28] K. Binder and A. P. Young, *Rev. Mod. Phys.* **58**, 801 (1986).
- [29] O. Knop, G. Demazeau, and P. Hagenmuller, *Can. J. Chem.* **58**, 2221 (1980).
- [30] W. Verscharen and D. Babel, *J. Solid State Chem.* **24**, 405 (1978).
- [31] L. Cai and J. C. Nino, *Acta Cryst.* **B65**, 269 (2009).
- [32] J. N. Reimers, J. E. Greedan, and M. Björgvinsson, *Phys. Rev. B* **45**, 7295 (1992).
- [33] A. Sadeghi, M. Alaei, F. Shahbazi, and M. J. P. Gingras, *Phys. Rev. B* **91**, 140407 (2015), arXiv:1407.0849 [cond-mat.str-el].
- [34] K. Dwight and N. Menyuk, *Phys. Rev.* **119**, 1470 (1960).
- [35] G. B. Jensen and O. V. Nielsen, *J. Phys. C: Solid State Phys.* **7**, 409 (1974).
- [36] A. P. Ramirez, G. P. Espinosa, and A. S. Cooper, *Phys. Rev. Lett.* **64**, 2070 (1990).
- [37] J. T. Chalker, P. C. W. Holdsworth, and E. F. Shender, *Phys. Rev. Lett.* **68**, 855 (1992).
- [38] I. Ritchey, P. Chandra, and P. Coleman, *Phys. Rev. B* **47**, 15342 (1993).
- [39] J. W. Krizan and R. J. Cava, *Phys. Rev. B* **92**, 014406 (2015).
- [40] J. W. Krizan and R. J. Cava, *J. Phys.: Condens. Matter* **27**, 296002 (2015).

Supplementary Information: Structure Refinement

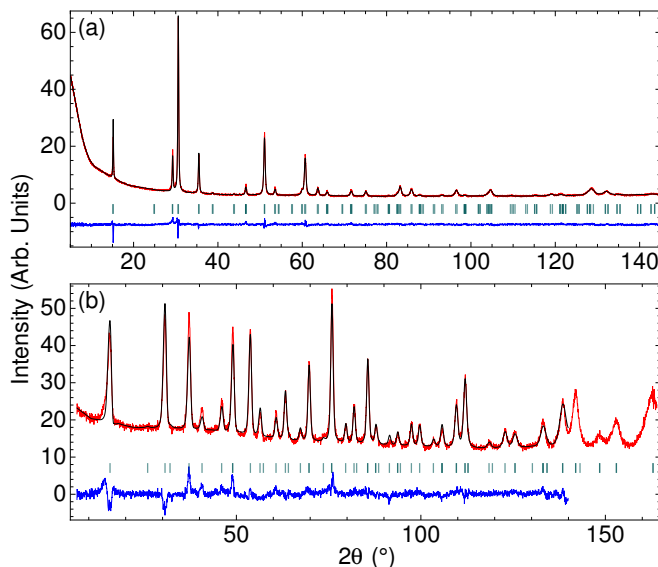


FIG. 6. Refined room temperature powder diffractograms for pyr-Mn₂Sb₂O₇: (a) x-ray and (b) neutron diffraction. Data are in red, the fit is in black, the residual is in blue, and vertical bars mark the calculated Bragg positions. The residual has been shifted for clarity.

Fig. 6 shows a joint refinement of x-ray and neutron powder diffraction data on pyr-Mn₂Sb₂O₇ at room temperature, in the $Fd\bar{3}m$ space group (# 227). The lattice parameter is $a = 10.1073(4)$ Å in the neutron data and $10.1205(11)$ Å in the x-ray data. The overall R -factors based on all points and not corrected for background were $R_p = 3.89\%$ and $R_{wp} = 5.00\%$ for the neutron pattern and $R_p = 2.98\%$ and $R_{wp} = 4.37\%$ for the x-ray pattern, with a global χ^2 of 0.757, based on 67 neutron reflections and 140/2 reflections for the x-ray pattern.

TABLE I. Refined atomic positions for pyr-Mn₂Sb₂O₇ in space group $Fd\bar{3}m$ (# 227) at room temperature.

Site	Mult.	x	y	z	B_{iso} (Å ²)
Mn	16d	0.5	0.5	0.5	2.85(16)
Sb	16c	0.0	0.0	0.0	2.11(10)
O1	48f	0.32744(16)	0.125	0.125	0.604(22)
O2	8b	0.375	0.375	0.375	0.604(22)

The high background in the neutron data is attributed to the presence of hydrogen — the material is prepared at relatively low temperatures from a hydrate and an organic Mn source, both of which are rich in H atoms, and takes the form of an extremely fine powder with a high surface-to-volume ratio and considerable potential to host adsorbed water. In analyzing this sample, the Mn site was allowed to deviate from full occupancy as a test for Mn vacancies. The x-ray refinement was not improved — the refined Mn content was 1.99(5), indicating full occupancy. However, the joint refinement suggested vacancies on the Mn and Sb sites when the occupancy of each was allowed to vary, and excess scattering on the O1 site in particular. This may indicate the presence of remnant hydrogen atoms, but without a model for what species would be present (*e.g.*, H₂O, H₃O⁺), we were not able to reach firm conclusions. The refined structure of pyr-Mn₂Sb₂O₇ is summarized in Tab. I, and selected bond lengths and bond angles that may be of particular interest for the magnetic interactions are presented in Tab. II.

TABLE II. Selected bond lengths and bond angles for pyr-Mn₂Sb₂O₇ at room temperature, based on the refinement presented in Fig. 6 and Tab. I.

Sites	Bond length	Bond angle
Mn–O1	2.5001(8) Å	
Mn–O2	2.19115(14) Å	
Sb–O1	1.9532(7) Å	
Mn–O1–Mn		91.38(4)°
Mn–Mn	3.5781(3) Å	